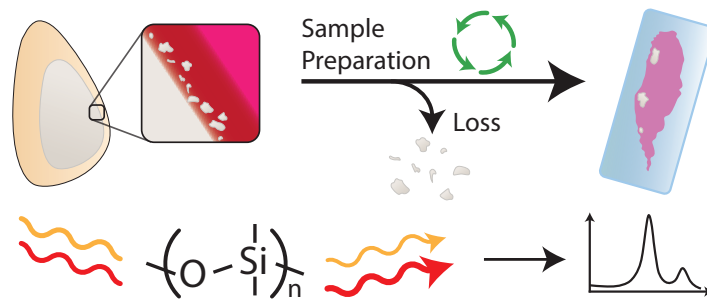


# Silicone loss during histological preparation of breast implant tissue from capsular contracture, quantified by Stimulated Raman Scattering microscopy

Robert W. Schmidt<sup>1</sup>, Erik de Bakker<sup>2</sup>, and Freek Arie<sup>1</sup>

<sup>1</sup>LaserLaB, Vrije Universiteit Amsterdam

<sup>2</sup>Departments of Molecular Cell Biology and Immunology, and Plastic, Reconstructive and Hand Surgery, Amsterdam UMC, Location VUMC



## Research highlights:

- Stimulated Raman scattering microscopy was used to quantify PDMS in silicone breast implant capsules.
- Two different histological processes (snap-frozen vs. paraffin-embedded) were applied to adjacent tissue slices.
- About 5x more silicone was found in snap-frozen prepared silicone implant capsule samples.
- Losses are likely to result in an underestimation of the actual silicone levels in paraffin embedded samples.

## Keywords:

Stimulated Raman Scattering, silicone, capsular contracture, tissue preparation

## Abstract

Breast augmentations, commonly performed for aesthetic or medical reasons, often use silicone (PDMS) implants. Some patients develop complications like capsular contracture, where scar tissue forms around the implant. Previously, we used stimulated Raman scattering (SRS) microscopy to detect and quantify silicone in stained capsule tissue, finding a correlation between silicone amount and contracture severity. However, we suspected silicone loss during histological preparation, which includes multiple steps like formalin fixation and paraffin embedding. In this study, we assessed silicone loss by comparing adjacent tissue samples from the same capsule: one prepared conventionally and the other snap-frozen. SRS microscopy revealed that snap-frozen samples had roughly five times more silicone, indicating significant silicone loss during conventional preparation. Thus, measuring silicone in histologically prepared samples likely underestimates PDMS content.

## 1 Introduction

Breast implant surgery is the one of the most common plastic surgery performed worldwide, with an estimated 1.7 million procedures in 2021 and 2.2 million in 2022, according to self-reported numbers by surgeons surveyed by the American Society of Plastic Surgeons [1, 2]. These augmentations are performed by fat transfer or through silicone implants filled with saline or silicone gel [2].

Complications after breast implant surgery have been the subject of substantial academic and public interest. They include but are not limited to, capsular complaints (contracture), breast implants-associated anaplastic large cell lymphoma (BIA-ALCL) and breast implant illness [5, 7]. The implant itself, or bleeding/leaking of silicone into the surrounding tissue is thought to play a role in all these conditions [7, 11, 13]. It is now common practice to advise revision or replacement of the implants at regular intervals [3].

A selective and sensitive detection technique for silicone in tissue is essential for research into the role of silicone in the pathophysiological processes involved in all the silicone-associated complications of breast implant surgery. Silicone gel implants are made of medical grade polydimethylsiloxane (PDMS), often called silicone, which is a chemically inert and thermally stable material [11]. The implant hull consists of elastic silicone rubber, while the filling is made of viscous silicone gel. PDMS molecules are made up of an alternating backbone chain of inorganic silicon (Si) and oxygen, with two methyl groups attached to each silicon atom. The length of the polymer chain also influences the viscosity of the PDMS. The precise silicone recipe and the production process are closely guarded secrets by each manufacturer. However, the rough production process is described in the literature [6, 11, 21]. Implant shells are produced by immersing an implant-shaped template for several seconds in a bath of liquid silicone that also contains fillers that increase the stiffness, electrical conductivity or radiopacity of the shell. Subsequently, the evenly coated templates

are cured in a laminar flow oven at high temperatures, which creates a silicone elastomer shell with highly 3D cross-linked polymers. This is repeated several times until the implant shell consists of 4 - 10 layers, depending on the manufacturer's specification. Research has shown that implants with a textured surface are less prone to developing stiff fibrous capsules around the implant [4]. A rough implant surface is created by dipping the implant in salt crystals between the silicone bath and the curing step. After the curing process, the salt crystals are removed by washing the implant, leaving a textured surface behind. The implants are filled with PDMS of different viscosities. The foundation structure is given by a lightly cross-linked silicone gel, which is swollen by short-chain silicone fluids to give the implant the desired cohesiveness. This means that the silicone fluid can move freely within the lightly cross-linked silicone network. To retain silicone fluid within the implant, the inside of the implant shells is coated with silicone rubbers that contain phenyl ( $C_6H_5$ ) or trifluoropropyl ( $CF_3CH_2CH_2$ ) groups. However, cases in which the coating does not fully prevent bleeding of PDMS through pores in the silicone rubber shell are known [18].

Various analysis techniques exist that can detect the PDMS polymer or its main component, silicon (Si) in biopsies. For example, elemental silicon was quantified in the breast and capsular tissue of silicone implants by inductively coupled plasma atomic emission spectroscopy [15]. This sensitive method is capable of determining trace element concentrations, but it is also a destructive method, since tissues are digested with acid for analysis, thus losing spatial information over the silicone locations and distribution. Energy-dispersive X-ray (EDX) analysis has been used as a qualitative method to identify silicon. However, it was used only at a few locations in histological prepared tissues to confirm the presence of elemental silicon [12, 23]. Kappel et al. combined EDX with a dye called Oil Red O to stain PDMS in organs and breast capsules [12, 18] and qualitatively demonstrated with EDX that the Oil Red O dye stained silicone particles. However, this dye also binds to neutral fats, fatty acids, and triglycerides and is therefore not a silicone gel-specific dye [8, 22]. Infrared microspectroscopy has been used to scan implant capsules for PDMS but has a physically limited spatial resolution [14]. Furthermore, infrared light is absorbed by glass, thus making the method not compatible with standard histopathology microscopy glass slides. Instead, tissues must be prepared on costly  $CaF_2$  substrates for IR measurements.

As an alternative to IR spectroscopy, Raman spectroscopy is an analytical technique that measures the vibrational energies in a molecule. This is done by sending a laser with a narrow wavelength onto a sample; the laser photons can be absorbed by the molecule or re-emitted at the same wavelength, which is called elastic scattering. In rare cases, the photon is scattered at another wavelength (inelastic scattering), and the energy shift of the scattered photons corresponds to the vibrational modes in the molecule, which are unique for every molecule and can be used to identify compounds. Although Raman spectroscopy is a nondestructive method able to measure tissues fixed on standard microscopy glass slides, it is also a slow method, especially when

scanning tissues at submicrometer resolution. Stimulated Raman Scattering (SRS) microscopy overcomes this shortfall by increasing the measuring speed by a factor of 3-5 orders of magnitude, making it possible to scan a tissue for PDMS within a reasonable time. [25] However, instead of acquiring a detailed Raman spectrum for each location, narrow-band SRS can scan only at one wavenumber at a time and is therefore limited to carefully chosen wavenumbers. SRS is a technique that uses two pulsed lasers in the near-infrared region; one is used to excite the molecule to a virtual energy state (Pump), while the other laser is used to stimulate a specific vibrational transition in the molecule (Stokes). A stimulated emission signal is generated when the difference in frequency between those lasers matches that of a vibration in the molecule of interest at the focal spot of the two lasers. The Stokes laser gains energy (intensity) through the stimulated emission of photons, whereas the pump laser loses energy. This energy transfer between the lasers is only a very small fraction of the intensity, but can be measured by modulating one of the lasers (in our case the Stokes beam) and using a lock-in amplifier for detection of the intensity fluctuations in the pump signal.[9, 19] These stimulated transitions result in a stronger signal, which means that the exposure time per pixel can be reduced to microseconds instead of seconds with conventional spontaneous Raman scattering. Importantly, the SRS signal can only be generated if both pulsed lasers overlap in time and space within the sample, which improves the measurable z-resolution in the sample dramatically.[20] Furthermore, SRS distinguishes itself from spontaneous Raman spectroscopy by suppressing the fluorescence signal, which can arise from sources such as glass, glue, or autofluorescence, and often obscures the Raman peaks in conventional Raman mapping [10].

Silicone fluids are highly soluble in hydrocarbon solvents (toluene, xylene), mineral spirits, and chlorinated hydrocarbons, but are not soluble in water (hydrophobic). The tissue comes into contact with different solvents during the paraffin embedding process (fixation, dehydration, and defatting). In addition, the sliced tissues are transferred onto a microscopy slide through a flotation water bath, which leads to the belief that silicone could be washed off the tissue during each of these processing steps. Kappel et al. already suggested in their research that paraffin preparation can dissolve some of the silicone [12]. However, the degree of silicone loss during fixation and paraffin embedding was never investigated.

In this study, we determine the extent of possible silicone loss during standard histological sample preparation; formalin fixation, paraffin embedding, and cutting. We selected tissues that we expected to contain uniformly distributed amounts of deposited silicone from bleeding implants. In a previous study, we already found a correlation between silicone concentration in capsule tissue and the severity of capsular contracture by comparing samples from patients with bilateral implants but unilateral contracture [7]. For the current study, we selected capsule tissue from patients with severe capsular contracture (Baker IV) and processed the tissues in two ways. One piece of the capsule was prepared by paraffin embedding, while the adjacent piece of the capsule

was prepared by snap-freezing. Snap freezing avoids the many washing steps of paraffin embedding in which silicone particles could be lost. We measured both paraffin-embedded and snap-frozen tissues with Stimulated Raman Scattering Microscopy because of its non-destructive nature, fast acquisition, and high chemical specificity to determine silicone levels in the tissues.

## 2 Methodology

### 2.1 Stimulated Raman Scattering microscopy

Stimulated Raman scattering microscopy images were captured with a custom-built system as previously described [10] and can be found in the supporting information, A.1. Two scans per tissue were obtained, one at a wavenumber that exhibits a strong Raman peak from the methyl groups ( $\text{CH}_3$  stretch) of PDMS and one where no PDMS signal is present. The corresponding wavenumbers are  $2905\text{ cm}^{-1}$  for silicone and  $2933\text{ cm}^{-1}$  for the "tissue background" [10]. The pixel step size for all measurements was  $1.62\text{ }\mu\text{m}$  and the powers under the microscope were set at 7 mW for the Pump and 14 mW for the Stokes beam. This power ratio of 1:2 for the Pump and Stokes was recommended by Moester et al. [16]. The images were acquired with a pixel dwelltime of 100  $\mu\text{s}$  which allows to scan one square centimeter ( $\text{cm}^2$ ) in about 1 hour at one wavenumber. A detailed description of the SRS setup and the data processing is reported in the SI.

### 2.2 Tissue preparation protocol

Adjacent samples were cut from a representative region of the entire explanted capsules and subsequently either taken for regular tissue preparation in paraffin or snap-frozen in liquid nitrogen and stored at  $-80^\circ\text{C}$ . Samples intended for regular preparation were fixed in a 4% formaldehyde solution for at least 24 hours. At the pathology department, these samples were processed routinely using a TissueTek VIP 6 (Sakura). In short, this involves a dehydration cycle with increasing ethanol concentration; 70%, 80%, 96% and three iterations of 100% ethanol, each one hour long at  $35^\circ\text{C}$ . Next, a cleaning cycle of three iterations with xylene of one hour long at  $35^\circ\text{C}$ . Finally, three-hour impregnating cycles at  $63^\circ\text{C}$  in paraffin. Samples were then embedded in paraffin before 5 to 30  $\mu\text{m}$  sections were cut using a microtome. The sections were transferred to a glass slide. The samples were then used without further processing.

Snap-frozen samples were cut into 5 or 50  $\mu\text{m}$  sections using a cryostat (CryoStar NX70, Fisher Scientific). After air-drying for 10 minutes they were covered using cryomatrix embedding resin (Eprexia, Fisher Scientific) and fixed between a glass slide and a coverslip.

### 2.3 Ethics

Clinical grading, the explantation of implants and the collection of capsules were performed by an experienced plastic surgeon (FBN) and samples were included only after oral informed consent. Tissue samples were collected in compliance with the ‘Code for Proper Secondary Use of Human Tissue’ as formulated by the Dutch Federation of Medical Scientific Organization. This study was performed per the Declaration of Helsinki and the guidelines for Good Clinical Practice.

## 3 Results and Discussion

The tissues of two Baker IV capsules (severe contraction) were divided into three pairs and adjacent slices were prepared snap-frozen or embedded in paraffin and microtomed. In total, 31 tissues were analysed, of which 14 were snap frozen and 17 were embedded in paraffin. Using SRS microscopy, silicone particles were found in 12 out of 14 snap-frozen slices and in 9 out of 17 paraffin-embedded tissue slices.

During the inspection of the generated PDMS abundance maps, it became clear that the silicone particles were located close to the edge on one side of the tissue, which had been adjacent to the silicone implant. Furthermore, the particles in paraffin-embedded slices seemed to be more clustered than in snap-frozen samples. Figure 1 shows typical example shapes of selected silicone particles in snap-frozen (A-C) and paraffin-embedded (D-F) samples. These silicone particles can be described as small single thin needle-shaped fibers with rounded edges or large objects that appear to consist of multiple intertwined particle clusters. Furthermore, in the paraffin-embedded images, the paraffin and tissue are also visible, showing that the silicone particles are enclosed by collagen fibers next to the edge of the tissue.

In total, 36 particles were detected in 14 snap-frozen samples with a median size of  $291 \mu\text{m}^2$ , a lower quartile of  $174 \mu\text{m}^2$  and upper quartile of  $1155 \mu\text{m}^2$ , as seen in Figure 2. The smallest particle had a size of  $40 \mu\text{m}^2$  and the largest particle had a size of  $5949 \mu\text{m}^2$ . The paraffin-embedded sample contained 22 particles with a median size of  $582 \mu\text{m}^2$ , the lower quartile was at  $220 \mu\text{m}^2$  and the upper quartile at  $1331 \mu\text{m}^2$ . The smallest particle found had a size of  $43 \mu\text{m}^2$  while the largest had a size of  $2202 \mu\text{m}^2$ . Expressing the number of particles found in tissues per area, we found 31.0 particles per  $\text{cm}^2$  in snap-frozen tissues and 6.8 particles per  $\text{cm}^2$  in paraffin embedded tissues.

Due to the different sample sizes in our study, we quantified the silicone concentration in relation to the total area of the tissue (excluding the fixation matrix / paraffin). This relative area is expressed here in ppm:  $\mu\text{m}^2$  of silicone area per  $\text{mm}^2$  of tissue area. In the three snap-frozen tissues samples an average area silicone concentration of 254, 302, and 270 ppm was found, whereas in paraffin-embedded tissues we detected 31, 7 and 167 ppm of silicone, as seen in Figure 3.

Overall, these results indicate that the snap-frozen prepared tissues con-

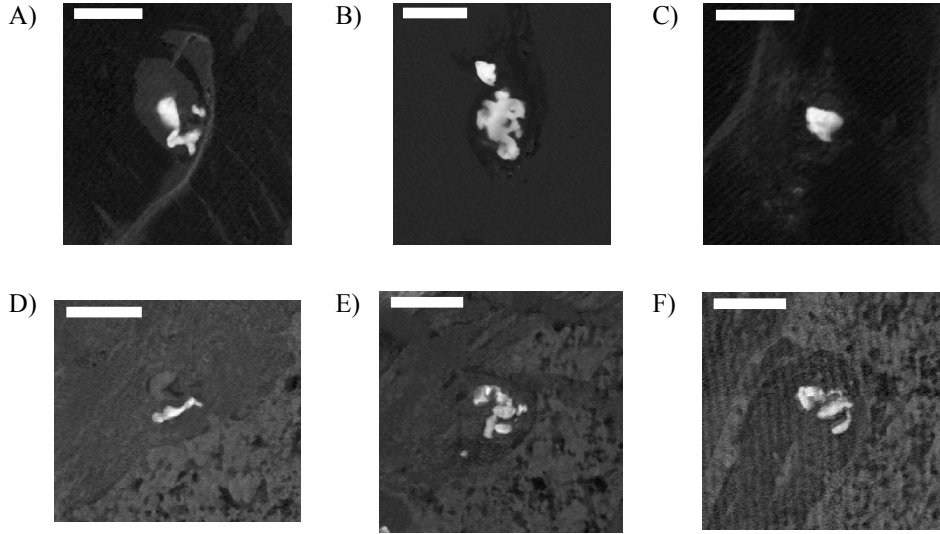


Figure 1: Selection of silicone specific abundance maps acquired by Stimulated Raman Scattering microscopy of selected locations from the third biopsy. Silicone particles are visible as bright objects in the Snap-frozen (A-C) and paraffin-embedded (D-F) tissue slices. Furthermore, in the paraffin-embedded images the paraffin matrix and tissue structures are visible. Scalebar 100  $\mu\text{m}$

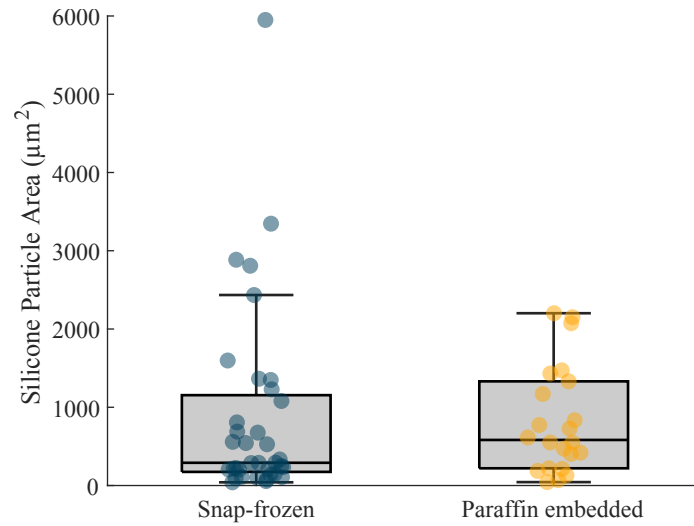


Figure 2: Particle sizes of silicone found in breast implant capsules that were histologically prepared by snap-freezing and paraffin embedding. The median particle area in snap-frozen tissues is 291  $\mu\text{m}^2$  and in paraffin-embedded is 582  $\mu\text{m}^2$

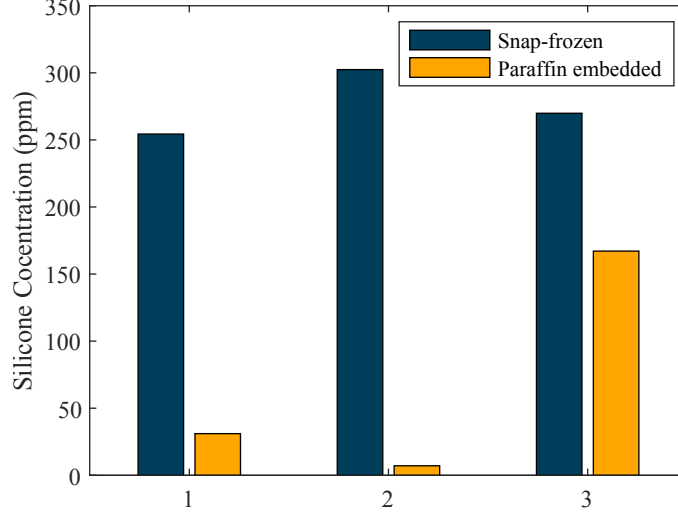


Figure 3: Concentration of silicone particles (area relative to the total tissue area) in snap-frozen prepared and paraffin-embedded tissues from three locations in Baker IV grade capsules.

tained many more particles, both smaller and larger, compared to the paraffin-embedded samples, see Figure 2. Furthermore, it was determined that silicone had a lower concentration in paraffin-embedded slices when comparing all tissue pairs, see Figure 3. This would suggest that small and large particles were washed out or reduced in size during the multiple processing steps of paraffin-embedding, with few medium-sized particles remaining in the tissue.

It should be mentioned that, given the study design based on adjacent samples, we assumed an even distribution of particles within the sample pairs; nevertheless, silicone "bleeding" or shedding is an uncontrollable naturally occurring process that could have led to uneven silicone concentrations between the analyzed tissue pairs.

Stimulated Raman Scattering microscopy is a fast and chemically specific method to identify polymers such as PDMS in samples. The spatial (x,y) resolution is  $0.67\text{ }\mu\text{m}$  [24], compared to other methods, makes it possible to measure the size and distribution of silicone debris in the samples. However, the SRS signal is only generated in the focal overlap between the Stokes and Pump beam, which we had previously determined to have a z height of  $2.6\text{ }\mu\text{m}$  [17]. The particles above or below the focal volume do not contribute to the SRS signal and will not be observed. In this study, we report the area of the particles compared to the area of the tissue to overcome uneven sample sizes.

During the SRS acquisition, we encountered transient absorption artifacts that showed up as individual bright pixels in the binary silicone image. To avoid falsely classifying these as silicone particles, we applied a connected component filter that removed particles with fewer than 5 connected pixels, corresponding with a lower size limit of 6 pixels ( $15.7\text{ }\mu\text{m}^2$ ). Furthermore, we used a GUI to manually check the classified silicone particles, which reduced the falsely classified silicone particle. However, this is a quite laborious method to overcome false positives due to subtraction artefacts, and could be solved

by scanning the sample with a third wavelength for silicone or background, which in turn would increase the scanning time by a factor of 1.5.

The most striking observation that emerged from the analysis based on the particle sizes and distribution was that large particles become smaller during histological preparation because of the partial removal of PDMS, whereas small particles dissolve and are no longer detected. This would explain the different concentration of silicone particle described in Figure 2.

## 4 Conclusion

Histopathological sample preparation by paraffin embedding, formalin fixation, and staining is the gold standard in the pathological field. However, during this procedure, the tissues are exposed to mechanical stress and washed several times with non-polar solvents to fixate, defat and dehydrate the tissue. Tissues containing unincorporated foreign material like PDMS from silicone implants are prone to losing these particles since the washing steps can remove or dissolve those particles.

The tissues of two Baker IV capsules (severe contraction) were divided into 3 pairs, and adjacent slices were prepared snap-frozen or embedded in paraffin and then analysed. On average, more silicone particles were found in snap-frozen than in paraffin-embedded tissues. Due to the different sample sizes in our study, we quantified the silicone area relative to the total area of the analysed tissues. In the snap-frozen prepared tissues, we found concentrations of silicone that were on average more than five times higher than in the paraffin-embedded tissue.

This research showed a loss of silicone particles during paraffin embedding that is commonly used before staining the tissue (e.g. H&E or MORO for silicone). Thus, a severe underestimation of the level of silicone debris is expected when paraffin-embedded samples are used to determine the extent of PDMS leakage.

## Acknowledgments

We would like to thank undergraduate students Nina van den Bergh and Jasmijn Rootlieb for their help in testing Matlab algorithms and scanning slides. Frank B. Niessen (FBN) for grading the capsular contracture according to the Baker scale.

This research received funding from the Netherlands Organisation for Scientific Research (NWO) in the framework of the ENW PPP Fund for the top sectors (Grant No. 741.018.202 ‘Soft Advanced Materials’) and from the Ministry of Economic Affairs in the framework of ‘PPS-Toeslagregeling’.

## Conflict of Interest

The authors declare that they have no known competing financial interests or personal relationships that could have appeared to influence the work reported in this paper.

## Contribution

**RWS:** Conceptualization, Methodology, Software, Formal analysis, Investigation, Writing- Original draft preparation **EB:** Conceptualization, Resources, Writing - Review & Editing **FA:** Conceptualization, Writing - Review & Editing, Supervision, Funding acquisition

## A Appendix Section

### A.1 Stimulated Raman Scattering Microscopy setup

A picosecond Lumera Plecter Duo Nd:YAG laser with a 1064 nm and a frequency-doubled 532 nm output was used. The 532 nm beam was used to pump a Levante Emerald Optical Parametric Oscillator (OPO), while the output 1064 nm beam was sent onto a delay stage and to an Acousto-Optical Modulator at 3.636 MHz from EQ Photonics GmbH. The OPO (Pump beam) was tuned so that the photon energy difference with the fixed 1064 nm beam (Stokes) would correspond with the targeted molecular vibration. Then both beams were spatially overlaid with the help of a dichroic mirror and sent to a Zeiss Examiner 7MP laser scanning microscope. We used a C-achroplan W 32x water immersion objective with a numerical aperture of 0.85 and a water immersion condenser with a numerical aperture of 1.2. The 1064 nm beam was blocked by a filter and the pump beam intensity was measured to reveal the stimulated Raman loss signal. For detection, we used a DET36A photodetector from Thorlabs, and the signal was demodulated with a lock-in amplifier from Zurich Instruments. SRS scans were acquired through Zeiss’s proprietary ZEN2011 microscope software with a step size of 1.62  $\mu\text{m}$ , a pixel dwell time of 100  $\mu\text{s}$ .

## A.2 Data processing

Data processing of the acquired SRS images was performed in MATLAB R2021a. The tissue area was determined by creating a tissue-specific mask by applying a graph cut function that classifies the tissue and the background pixels. The vacuoles in the tissue were also counted as tissue area, and the mask was closed with MATLAB’s fill-hole function. Burn or transient absorption artefacts from the SRS measurements can hinder the data analysis because they appear in the SRS images as extremely dark or bright pixels. These pixels are identified by calculating the three-times standard variation of the pixel intensity and are removed by replacing them with median smoothed pixels from the neighborhood (3x3). Subsequently, the pixel intensities of the background SRS image were adjusted to that of the silicone image intensity to compensate for variations in laser power between the image acquisitions. A silicone-specific image was created by subtracting the background scan from the silicone scan, and outlier pixels were removed with the same method as the burn and transient absorption artefacts. A threshold was applied to the image to create a binary silicone mask of the brightest pixels. Small particles in the binary mask that contained less than six connected pixels (min area  $16 \mu\text{m}^2$ ) were seen as possible artefacts and removed from the silicone mask. Each classified silicone particle was then visually inspected to reduce false positives by considering the shape of the particles, the pixel intensities in the SRS images, and the locations of the particles.

## A.3 Overview of particles per tissue

Table 1 and 2 show the number and area of silicone particles found in frozen frozen snap tissues and paraffin-embedded tissues, respectively. Each row corresponds to an analyzed tissue slice.

Capsule location	Tissue number	Number of particles in tissue	Area of silicone particles $\mu\text{m}^2$	Area of tissue in $\text{mm}^2$
1	1	0	0	5.98
1	2	10	7578	4.71
1	3	1	223	7.31
1	4	1	56	3.55
1	5	4	737	6.77
1	6	2	525	7.53
2	1	3	428	6.84
2	2	5	6147	14.90
3	1	2	3095	9.59
3	2	1	689	10.02
3	3	0	0	3.24
3	4	2	1708	14.45
3	5	2	7030	12.47
3	6	3	3241	8.64

Table 1: Overview of silicone particles found in snap frozen prepared tissues.

Capsule location	Tissue number	Number of particles in tissue	Area of silicone particles $\mu\text{m}^2$	Tissue area in $\text{mm}^2$
1	1	2	2143	25.63
1	2	1	550	9.38
1	3	0	0	25.71
1	4	0	0	24.64
1	5	1	773	27.73
1	6	2	1518	21.09
1	7	0	0	26.40
2	1	0	0	14.25
2	2	0	0	14.20
2	3	0	0	16.39
2	4	0	0	13.07
2	5	1	614	13.73
2	6	0	0	15.16
3	1	8	5125	12.35
3	2	4	3988	17.47
3	3	1	1472	22.82
3	4	2	1850.88	21.77

Table 2: Overview of silicone particles found in paraffin embedded tissues.

## References

- [1] ISAPS International Survey On Aesthetic/Cosmetic Procedures performed in 2021. Technical report, International Society of Aesthetic Plastic Surgery, 2022.
- [2] ISAPS International Survey On Aesthetic/Cosmetic Procedures performed in 2022. Technical report, International Society of Aesthetic Plastic Surgery, 2023.
- [3] American Society of Plastic Surgeons. Breast Implant Removal.
- [4] Olle Asplund, Leif Gylbert, Göran Jurell, and Christopher Ward. Textured or smooth implants for submuscular breast augmentation: a controlled study. *Plastic and reconstructive surgery*, 97(6):1200–6, 5 1996.
- [5] Yara Bachour, Stephan P. Verweij, Susan Gibbs, Johannes C.F. Ket, Marco J.P.F. Ritt, Frank B. Niessen, and Margriet G. Mullender. The aetiopathogenesis of capsular contracture: A systematic review of the literature, 3 2018.
- [6] Simon Barr and Ardeshir Bayat. Breast surgery review article: Breast implant surface development: Perspectives on development and manufacture, 2 2011.
- [7] Erik de Bakker, Liron Zada, Robert W. Schmidt, Ludo van Haasterecht, A. Dick Vethaak, Freek Ariese, Henry B. P. M. Dijkman, Peter Bult, Susan Gibbs, and Frank B. Niessen. Baker Grade IV Capsular Contracture Is Correlated with an Increased Amount of Silicone Material: An Intra-patient Study. *Plastic & Reconstructive Surgery*, 152(6):1191–1200, 12 2023.
- [8] S D Fowler and P Greenspan. Application of Nile red, a fluorescent hydrophobic probe, for the detection of neutral lipid deposits in tissue sections: comparison with oil red O. *Journal of Histochemistry & Cytochemistry*, 33(8):833–836, 8 1985.
- [9] Christian W. Freudiger, Wei Min, Brian G. Saar, Sijia Lu, Gary R. Holtom, Chengwei He, Jason C. Tsai, Jing X. Kang, and X. Sunney Xie. Label-Free Biomedical Imaging with High Sensitivity by Stimulated Raman Scattering Microscopy. *Science*, 322(5909):1857–1861, 12 2008.
- [10] Ludo Haasterecht, Liron Zada, Robert W. Schmidt, Erik Bakker, Ellis Barbé, Heather A. Leslie, A. Dick Vethaak, Susan Gibbs, Johannes F. Boer, Frank B. Niessen, Paul P. M. Zuijlen, Marie Louise Groot, and Freek Ariese. Label-free stimulated Raman scattering imaging reveals silicone breast implant material in tissue. *Journal of Biophotonics*, 13(5), 2 2020.

- [11] Rita M. Kappel, Antonius J. H. Klunder, and Ger J. M. Pruijn. Silicon chemistry and silicone breast implants. *European Journal of Plastic Surgery*, 37(3):123–128, 3 2014.
- [12] R.M Kappel, L.L. Boer, and H. Dijkman. Gel Bleed and Rupture of Silicone Breast Implants Investigated by Light-, Electron Microscopy and Energy Dispersive X-ray Analysis of Internal Organs and Nervous Tissue. *Clinical Medical Reviews and Case Reports*, 3(1), 1 2016.
- [13] Sepehr S. Lajevardi, Pratik Rastogi, Daniel Isacson, and Anand K. Deva. What are the likely causes of breast implant associated anaplastic large cell lymphoma (BIA-ALCL)?, 6 2022.
- [14] Mark A. Mandel and Donald F. Gibbons. The presence of silicone in breast capsules. *Aesthetic Plastic Surgery*, 3(1):219–225, 12 1979.
- [15] Joseph P. McConnell, Thomas P. Moyer, David E. Nixon, Paul L. Schnur, Diva R. Salomao, Thomas B. Crotty, Jeffrey Weinzweig, John B. Harris, and Paul M. Petty. Determination of Silicon in Breast and Capsular Tissue From Patients With Breast Implants Performed by Inductively Coupled Plasma Emission Spectroscopy. Comparison With Tissue Histology. *American Journal of Clinical Pathology*, 107(2):236–246, 2 1997.
- [16] M. J. B. Moester, Freek Ariese, and Johannes F. de Boer. Optimized signal-to-noise ratio with shot noise limited detection in Stimulated Raman Scattering microscopy. *Journal of the European Optical Society: Rapid Publications*, 10:15022, 4 2015.
- [17] Miriam J.B. Moester, Liron Zada, Bart Fokker, Freek Ariese, and Johannes F. Boer. Stimulated Raman scattering microscopy with long wavelengths for improved imaging depth. *Journal of Raman Spectroscopy*, 50(9):1321–1328, 9 2019.
- [18] Jessica C.R. Mustafá, Eduardo de Faria Castro Fleury, and Henry B.P.M. Dijkman. Case Report: Evidence of Migratory Silicone Particles Arising From Cohesive Silicone Breast Implants. *Frontiers in Global Women’s Health*, 3, 2022.
- [19] P. Nandakumar, A. Kovalev, and A. Volkmer. Vibrational imaging Based on stimulated Raman scattering microscopy. *New Journal of Physics*, 11, 2009.
- [20] Richard C. Prince, Renee R. Frontiera, and Eric O. Potma. Stimulated Raman Scattering: From Bulk to Nano. *Chemical Reviews*, 117(7):5070–5094, 4 2017.
- [21] Guillermo Ramos-Gallardo, Estela Vélez-Benítez, Jesús Cuenca-Pardo, Lázaro Cárdenas-Camarena, Arturo Ramírez-Montañana, Adrián Carballo-Zarate, Livia Contreras-Bulnes, Javier Bucio-Duarte, Martín Morales-Olivera, and Rufino Iribarren-Moreno. What is the Process for

- Breast Implant Manufacturing? Inside Eight Breast Implant Factories. *Aesthetic Plastic Surgery*, 44(6):2063–2074, 12 2020.
- [22] G. Riva, M. Villanova, L. Cima, C. Ghimenton, C. Bronzoni, R. Colombari, M. Crestani, S. Sina, M. Brunelli, A. D’Errico, U. Montin, L. Novelli, and A. Eccher. Oil Red O Is a Useful Tool to Assess Donor Liver Steatosis on Frozen Sections During Transplantation. *Transplantation Proceedings*, 50(10):3539–3543, 12 2018.
  - [23] O. Winding, L. Christensen, J. L. Thomsen, M. Nielsen, V. Breiting, and B. Brandt. Silicon in human breast tissue surrounding silicone gel prostheses: A scanning electron microscopy and energy dispersive x-ray investigation of normal, fibrocystic and peri-prosthetic breast tissue. *Scandinavian Journal of Plastic and Reconstructive Surgery and Hand Surgery*, 22(2):127–130, 1988.
  - [24] Liron Zada, Bart Fokker, Heather A. Leslie, A. Dick Vethaak, Johannes F. de Boer, and Freek Ariese. Stimulated Raman scattering simulation for imaging optimization. *Journal of the European Optical Society-Rapid Publications*, 17(1), 12 2021.
  - [25] Liron Zada, Heather A. Leslie, A. Dick Vethaak, Gerjen H. Tinnevelt, Jeroen J. Jansen, Johannes F. de Boer, and Freek Ariese. Fast microplastics identification with stimulated Raman scattering microscopy. *Journal of Raman Spectroscopy*, 49(7):1136–1144, 7 2018.